ESPL
Earth Surface Processes and Landforms

Introduction

Cavernous weathering (tafoni formation) is a classic example of a feature most likely attributable to multifactorial processes. Tafoni (singular, tafone) occur in hot and arid conditions (Campbell, 1999), coastal environments (Mottershead and Pye, 1994), and even in Antarctica (Strini *et al.,* 2008). Turkington and Paradise (2005) proposed detailed conceptual models of the evolution of tafoni in sandstones. They summarize the distribution as follows: '[...] They occur under cold, temperate, hot, humid and arid environments, and are found on a variety of rock types.' However, an arid period is generally considered necessary for tafoni development (Brandmeier *et al.,* 2011). The governing processes might be physical or chemical or a combination of the two (French and Guglielmin, 2000; Dorn *et al.,* 2013); various mechanisms such as salt weathering, dissolution, alternating wetting and drying, temperature fluctuations and aeolian processes have been proposed (Mol and Viles, 2012). Tafoni development can only be explained by a complex combination of processes (Turkington and Phillips, 2004), although many authors believe salt weathering to be the most important single process in many cases (Rodriguez-Navarro *et al.,* 1999; Brandmeier *et al.,* 2011) and moisture is often emphasized as a main driving factor (Mellor *et al.,* 1997).

To understand the development of tafoni, more data need to be collected on the environmental controls of the contributing weathering processes (e.g. salt weathering and hydration), in particular the temperature and moisture regimes and distribution of salts within tafoni and the surrounding rock. Our aim is to investigate the control parameters of tafoni formation in Tafraoute, Morocco, using an integrative approach which combines high-resolution temporal and spatial measurements of temperature, moisture and salt distribution. We aim to elucidate the small-scale interaction of temperature, rock moisture and salt levels and fluctuations that contribute to cavernous weathering in granite. Besides analyzing how, in the Tafraoute area, moisture and salts contribute to tafoni development, the field data can be used to underpin (or challenge) theoretical and mathematical models of tafoni formation.

Theories and Causes of Tafoni Weathering

Temperature and moisture regimes and salt distributions have all been proposed as important drivers of tafoni development. The effectiveness of 'pure' insolation or temperature weathering has been discussed for decades and will not be reviewed here in detail. In recent years, authors such as Hall and André (2001) and Hall *et al.* (2007) have pointed out that insolation is an underrated process and introduced the terms thermal fatigue and thermal shock. Rapid temperature fluctuations of $>2\ \mathrm{K\ min^{-1}}$ are regarded to be particularly important in causing rock breakdown, although the validity of this threshold has been recently challenged by Boelhouwers and Jonsson (2013). Nonetheless, there are still significant shortcomings in the availability of high-resolution temperature data (Sumner *et al.,* 2009). Temperature fluctuations in isolation have never been considered as the main agent of tafoni formation; but they might trigger moisture and salt movement. Two recent developments could contribute to novel datasets of temperature fluctuations within and outside tafoni: (1) the use of many cheap microsensors (iButtons); and (2) infrared thermography, which has, to our knowledge, never been reported on in a published paper on tafoni.

Moisture content in porous rock outcrops is extremely variable in time and space; quantitative assessment of moisture concentration is still challenging and there are few results from field sites. Most earlier field results were derived from weighing and drying samples (Hall, 1986, 1991). Matsukura and Takahashi (2000) measured moisture of sandstone blocks using an infrared moisture meter, while Eklund *et al.* (2013) tested and demonstrated the potential use of handheld capacitance and resitance-based moisture meters. For one or two decades geophysical techniques, such as 2D-geoelectrical measurements have been applied to natural rock (Sass, 2003, 2005; adapted by Mol and Viles, 2010) and the approach has been adapted to building stone using non-invasive adhesive electrodes (Sass and Viles, 2010a, 2010b) for monitoring moisture ingress into the stonework. Moisture distribution is commonly regarded as one of the most important determinants of tafoni formation (Mellor *et al.,* 1997) and moisture gradients may be crucial for the concentration of salts in certain topographic conditions (Huinink *et al.,* 2004). The application of borehole humidity sensors in this present investigation is a novel approach that has not been used before in this context.

Salts may derive from various sources (e.g. weathering of bedrock, road salts, atmospheric aerosols, capillary rise from groundwater, and coastal spray) and exert physical pressure on pore walls by thermal expansion, hydration, and crystallization (Goudie and Viles, 1997). They are a particularly important agent of weathering in arid, semiarid and urban environments and are considered highly important for tafoni evolution (Rodriguez-Navarro *et al.,* 1999). Salt weathering processes have been reviewed by Doehne (2002) and intensively investigated in the context of building stone deterioration and conservation (Maurício *et al.,* 2006; Dionisio *et al.,* 2013). A variety of different salts is thought to be involved in stone decay (Turkington *et al.,* 2003). A very heterogeneous distribution of dissolved salts within porous rock and stonework has to be considered in most environments. Capillary uptake of groundwater and atmospheric humidity are the main pathways by which salts enter rock and stonework (Martinho *et al.,* 2012). Thus, uptake of moisture and the behaviour of salt mixtures in the pores are mutually interconnected (Tsui *et al.,* 2003; Franzen and Mirwald, 2009).

Study Sites

The Anti-Atlas in southern Morocco is a Cambrian mountain belt running from NE to SW. Tectonic windows are found in this mountain belt in which Proterozoic rock complexes crop out. One of these windows is the Kerdous Massif in the western Anti-Atlas in which lies the Tasrirt Plateau at an altitude of 1000 m (Soulaimani and Piqué, 2004). Our study site is located on this plateau south of the small town of Tafraoute (GPS: 30°09′70″N; 09°13′15″ W). The predominant rock in the area is the Tafraoute Granite (Figure 1).

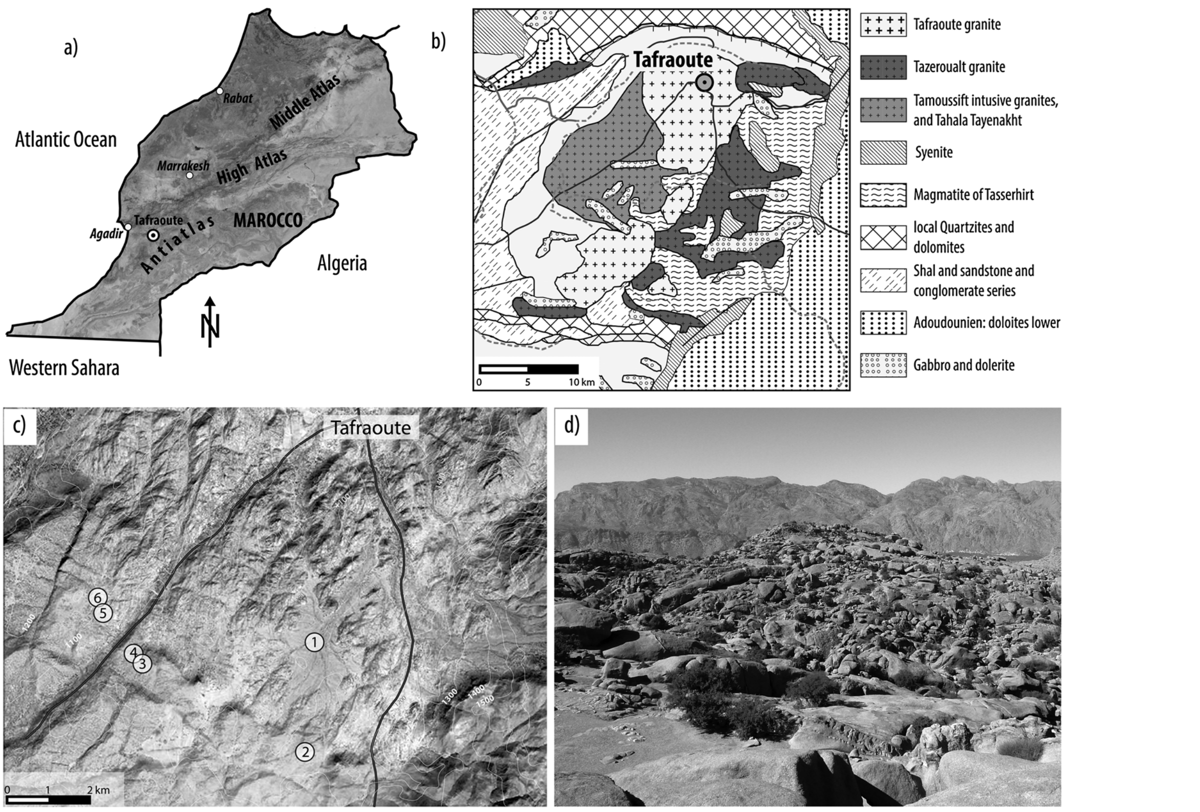

Figure 1. Overview of the study area. (a) location; (b) simplified geological map (taken from Service Géologique du Maroc, 1985); (c) location of the investigated sites in the study area; (d): impression of the granite landscape (taken from site 1 looking north).

In the field, the 550 million years old Tafraoute Granite is reddish-brown and rather coarse. Feldspar crystals of mm to cm size can be quite easily removed from the rough surfaces, and the rather low resistance to drilling (we drilled up to 50 cm deep with comparatively little effort) demonstrates that the rock is highly weathered in its entirety. This is confirmed by our own laboratory measurements: while typical textbook values for density of granite are between 2600 and 2800 kg m^{-3} and 0.4 to 1.5% for porosity (Materialarchiv, 2014), samples from the area showed a density of 2240 kg m^{-3} and a porosity of 8%. Details of the structural, geochronological and geochemical data on Tafraoute Granite can be found in Hassenforder (1985, 1987); Barbey *et al.* (2004) and Benziane (2007). In the granite landscape within an area of approximately 100 km^2, countless tafoni with different characteristics in terms of their shape, size and exposure occur especially on a number of tor-like outcrops. Pilot survey mapping revealed no specific distribution in terms of aspect or elevation. We chose six sites with tafoni of different sizes and shapes which are shown in Figure 2.

Owing to logistical constraints we focused most data collection on site 1 and in particular on the west-facing tafoni at this site. Owing to the completeness of the dataset obtained here, most of the results presented are derived from this site. Selected results from other sites are mentioned either to underpin the results of site 1 or to demonstrate deviations between sites.

There is no meteorological station directly in Tafraoute and so the climate parameters had to be estimated from different internet sources (Figure 3). As none of these sources give precise details on the origin of the data we only calculated the mean value for temperature and precipitation. Based on this calculation, Tafraoute has a mean annual air temperature of approx. 16°C. Precipitation is *c.* 250 mm yr^{-1} with a pronounced winter maximum (= BSk climate according to Köppen-Geiger). Frost may occur occasionally in winter nights. These figures broadly correspond to large-scale climate maps of Morocco. During the period of investigation

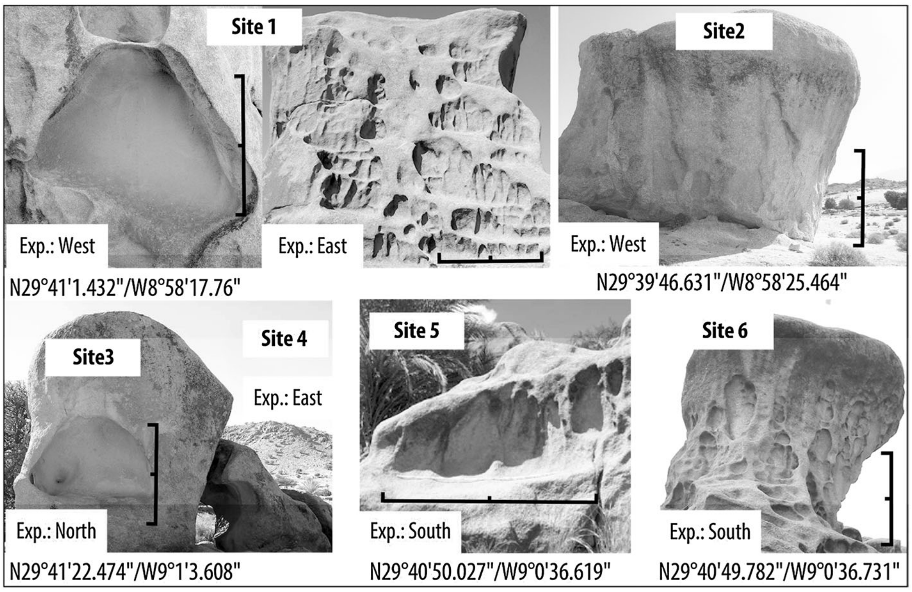

Figure 2. Representation of the different study sites; the black bar denotes 2 m.

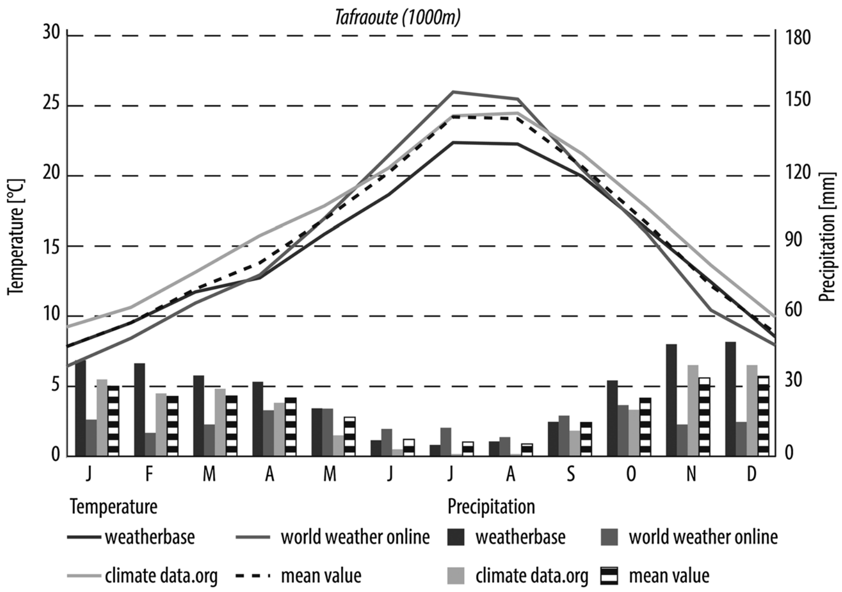

Figure 3. Climate in Tafraoute as derived from different internet sources (http://www.weatherbase.com/, http://www.worldweatheronline.com, ttp://en.climate-data.org).

(April 2014), air temperatures (measured with an iButton under an improvised radiation shield) ranged between 22.5 and 9°C.

Methodology

Fieldwork was carried out in February 2014 (during cool conditions in late winter). The investigations focused on the assumed basic parameters influencing tafoni formation: temperature, moisture and salts. The range of techniques used to investigate these three parameters and the measurements actually carried out at the six sites are compiled in Table I.

Infrared thermography

We used a VarioCam HR infrared camera with a thermal resolution of 0.03 K, an accuracy of ±1.5°C and a spectral range from 7.5 to 14 µm. The detector size is 640×480 pixels and can be increased to 1280×960 pixels by resolution enhancement technology. The spatial resolution at 5 m distance is 3 mm. For the basics of infrared thermography we refer the reader to Gaussorgues and Chomet (1993); Schuster and Kolobrodov (2000); Budzier and Gerlach (2010) and others. Applications of IR thermography to studies of rock walls are described by Teza *et al.* (2011). Emissivity is a key variable for thermography measurements and thus was determined in the field. To determine emissivity, one iButton measured air temperature and relative humidity and a second one the temperature of the rockwall within the sensor field of the IR camera. The air temperature data was then used to correct the evaluation software of the thermal images and the thermography data compared with the measurements from the iButton on the rock wall. The difference was compensated for by modifying the emissivity factor. Various measurements showed very similar results with a calculated emissivity value of 0.95. Similar results have been published by Gruner (2004); Shannon *et al.* (2005) and Testo (2006).

Surface temperatures were measured on three consecutive days for 24 h using a measurement interval of 10 min across the entire surface of three sides of the site 1 rock tor (E, W and S-facing). The aim of using this method was to derive daily average values of different micro-sites, temperature fluctuations and the possible impact on moisture transfer processes. The parameters were modified according to the calculated emissivity of 0.95.

Moisture meter

A handheld moisture meter (Voltcraft MF-100) was used to determine the moisture in the near-surface area both within and adjacent to selected tafoni. The capacitance sensor is commonly used for detecting water damage in buildings; its electrical field penetrates some 2–4 cm into the rock. The sensor can be used in geomorphology to assess semi-quantitative moisture distributions on reasonably smooth and sound surfaces (Eklund *et al.,* 2013). Detailed descriptions on the technical background can be found in James (1963) and Skaar (1988). The measurement points were arranged in the form of a grid with a mesh size of 25 cm at the respective sites; the total area of the grid depended on the micro-topographic conditions at each site (usually 10 × 10 measurements). The experimental design was to measure pairs of grids – one inside and one outside each tafoni – but lack of smooth and round surfaces outside sometimes precluded this. To reduce uncertainties, each point was measured three times. The final value was the mean of the three measurements. The aim was to get an overview of relative moisture distribution across the near-surface zone.

I-buttons

Miniature loggers (iButton Hygrochron™ DS1923) with 17.35 mm diameter were used to measure temperature and relative humidity (accuracy 0.5°C and 0.5%). At site 1, two sensors were attached to the surface inside the tafoni (one in the upper third, one in the lower third) and a reference sensor was positioned on the outside rock wall. In addition, the temperature conditions inside of the rock were determined by Thermochron DS1922L iButtons inserted into 3, 25, and 50 cm deep bore holes, each 18 mm diameter. Humidity was measured only at 3 cm and 50 cm with the exception of site 1 (east) where moisture was also determined at 25 cm depth for a period of four days (20/02/14 to 24/02/14). The Hygrochron buttons measure air humidity through a small hole at the top of the metallic housing. For that reason, a second borehole (6 mm in diameter and 5–8 mm longer) was drilled into the lower end of each hole (see Figure 4). This was to provide a confined air space to measure borehole humidity, in equilibrium with the surrounding rock moisture. The principle is based on the sorption isotherm (Franzen and Mirwald, 2009), the line of equilibrium moisture between air and rock in porous bodies at a certain temperature (see also Krus, 1995 and Plagge *et al.,* 2006). The iButtons were

Table I. Summary of measurements performed at the investigation sites.

	iButtons (surface)	iButtons (temperature profiles, 3 depths)	iButtons (moisture profiles, 2 depths)	IR Cam 24-hr monitor.	moisture meter grids	ERT profiles	Sampling drillholes
site1W	**1**	**1**	**1**	**1**	**2**	**10***	**4**
site 1E	—	1	**1**	1	**1**	1	1
site 1S	1	1	1	1	—	1	—
site 1N	—	1	1	—	—	—	—
site 2W	—	1	—	—	1	1	—
site 2E	—	—	—	—	—	1	1
site 3	—	—	—	—	**2***	**3****	**2**
site 4	—	—	—	—	1	**2****	—
site 5	—	1	1	—	—	—	—
site 6	—	1	1	—	—	—	—

At site1E measurements were also made at 25 cm for a short period (20/2/2014–24/2/2014).
Bold numbers: measurements presented in this paper.
*Only two profiles displayed;
**Only one profile displayed;

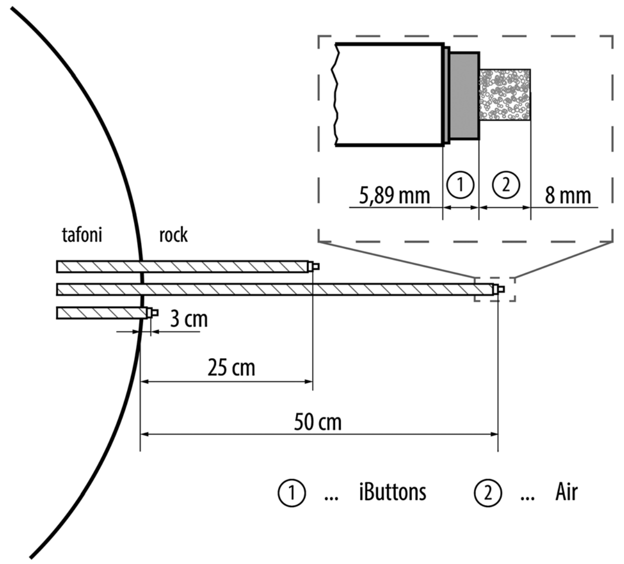

Figure 4. Setup for temperature and relative humidity measurements at different depths. Hatching: wooden rod, gray: iButton.

glued to a wooden rod to insert them into the boreholes and the narrow space between rod and rock was sealed at the surface with silicone paste. In fact, the rods fit so tightly into the drillholes that one of them could not be recovered and we thus assume that humidity transport along the rod is negligible. A similar setup of one Thermochron (25 cm depth) and two Hygrochrons at 3 cm and 50 cm depth was also installed at three further sites (additional to the four different orientations at site 1). Measurements were recorded at intervals of three min over the period between 14/02/14 and 24/02/14. Data loss occurred due to vandalism and theft, therefore, no data exist for some of the sensors from 19/02/14 to 21/02/14. At the main site 1 (west), 7 days of continuous measurement are available (14/02–19/02 and 21/02–24/02). Rock moisture values were calculated from the humidity data based on the sorption isotherm (Figure 5), which was determined in a climate chamber.

Electrical resistivity tomography

Electrical resistivity tomography (ERT) is a widely used geophysical tool for subsurface surveys and has been adapted for small-scale investigations on rock walls and building stone facades over the last decade (Sass, 2005; Mol and Viles, 2012). ERT is a geophysical profiling technique which detects zones of different electrical conductivity, usually along 2D-sections (for the principles we refer readers to Schrott and Sass, 2008). In the environment of weathered rock, different electrical properties are generally caused by heterogeneous water content and/or salt concentration. However, without the aid of further techniques, it is currently not possible to differentiate whether zones of high resistivity are caused by high water content, soluble salts, or a combination of both. We used a Geotom device equipped with 50 electrodes. On the relatively smooth surfaces within the tafoni, self-adhesive medical ECG-electrodes were used to establish electrical contact to the rock. Outside of the tafoni the surfaces were generally rougher and more friable and adhesive electrodes did not work properly; thus, we used metal screws temporarily inserted in small boreholes. On the backwall of the large west-facing tafoni at site 1, two profiles were measured: a vertical one from the bottom to the roof and a horizontal one about half way up. Electrode spacing was 6 cm resulting in total profile lengths of 2.94 m. Both profiles were measured every 6 h over a 24 h period (19/2/14–20/2/14). ERT profiles of similar configuration were measured at most of the other sites as well, but solely single measurements without 24 h monitoring.

2D-resistivity sections were calculated using the software package Res2Dinv (Geotomo Software, Penang, Malaysia). We tested the standard least-square inversion as well as robust inversion and compared both in order to verify the shape of detected anomalies. The measurement setups used were Wenner and dipole–dipole (Kearey et al., 2002) which allow good resolution of surface-parallel layers (Wenner) and of lateral inhomogeneities (dipole–dipole), respectively. Both arrays were combined in Res2Dinv to benefit from the advantages of both measurements. We checked the results of the calculation with the depth of investigation (DOI) method (Oldenburg and Li, 1999; Marescot *et al.,* 2003). The DOI is an empirical method for determining the depth down to which the results are considered trustworthy, and model regions with DOI index values >0.2 are usually considered unreliable in terms of their modelled absolute resistivity values (Hilbich *et al.,* 2009; Angelopoulos *et al.,* 2013).

Drilling and salt sampling

Sampling for salts was carried out by incrementally collecting the ample drilling dust from the installation of the iButtons and from further drillholes. This approach made it possible to sample at a range of depths and thus, to assess the concentration and the types of salts at different depths. At site 1, four drill holes were sampled; three inside the west-facing tafone (top, mid, bottom) and one from the open rock face beside the tafone. The samples were taken from the following six depth

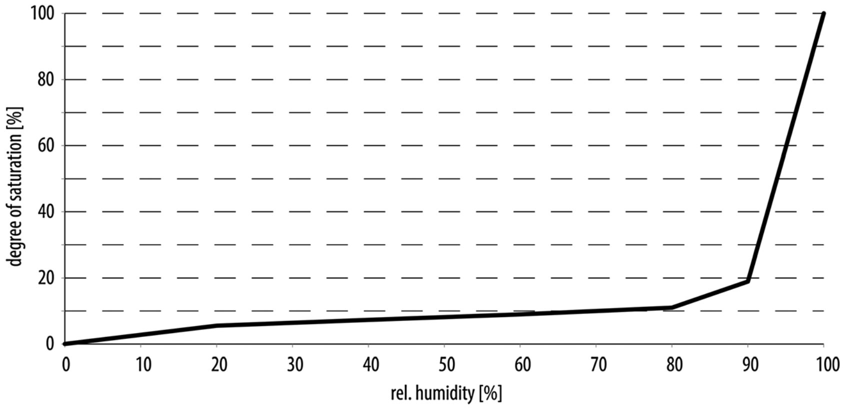

Figure 5. Sorption isotherm of the Tafraoute granite as derived from lab measurements.

increments: 0–2.5 / 2.5–5 / 5–10 / 10–15 / 15–20 / 20–25 cm. Analyses were performed in the Oxford Rock Breakdown Laboratory with the Ion Chromatography System Dionex IC DX500.

In addition to ion chromatography, a simple conductivity measurement was performed for each sample (1 g of drill dust dissolved in 5 mL of deionized water). The aim of this was to provide a quick assessment of overall salt concentration. The applied instrument was a bench-top conductivity meter (HI2315).

Results

Presentation of the results focuses on the west-facing tafone at site 1 (shown in Figure 2) because of the completeness of the datasets collected there. All of the following results refer to the inside of this tafone if not specified otherwise.

Infrared thermography

Data were collected every 10 min over an extended period (24 h), each measurement covering several m^2 with a spatial resolution of 3 mm. In Figure 6(a), the result of the averaging of all measurements is shown. It is obvious that the inside of the tafone is warmer on average than the surrounding rock surface. Furthermore, a significant temperature difference occurs between the bottom and the top of the tafone, whereas the surrounding rock surface shows more homogenous conditions. Figure 6(b) shows a horizontal and a vertical profile (along the lines indicated in Figure 6(a)) to illustrate this point. While there is almost no temperature difference in the horizontal-profile (blue line), a significant temperature decrease towards the bottom can be detected in the vertical profile (red line). The temperature difference is almost 3°C.

In Figure 6(c) the diurnal temperature cycles at defined positions (as marked in Figure 6(a)) are displayed. The selected positions can be divided into three areas: area one includes positions 1 to 8 (outside the tafone, green lines), area two includes positions 9 to 15 (upper inside area of the tafone, red lines) and area three includes positions 16 to 24 (lower inside area of the tafone, blue lines). The respective mean values for each area were calculated (Figure 6(d)). Area one (outside the tafone) shows the biggest amplitude and therefore the lowest (~3°C) and the highest (~20°C) values during the day. In the curves of areas two and three the maximum and minimum temperatures are subdued. Interestingly, the two curves run almost parallel to each other with the lower tafone being constantly cooler than the upper tafone. This effect cannot be caused by stronger emission at night (otherwise, the amplitudes would be higher); the most probable explanation is higher moisture content towards the base (see discussion). On the east side of site 1 the tafoni are much shallower and further away from the ground; accordingly, similar patterns were not recorded at this site (not displayed).

Moisture meter

As pointed out in the methodology section, this method can only be used to infer relative moisture distributions within the near-surface zone (0–4 cm) as the reliability for quantitative results is rather low (Eklund *et al.*, 2013). At the east-facing side of site 1, it was found that small, decimeter-scale tafoni are consistently wetter than the unweathered surrounding rock (Figure 7(c)). On the backwall of the large west-facing tafone

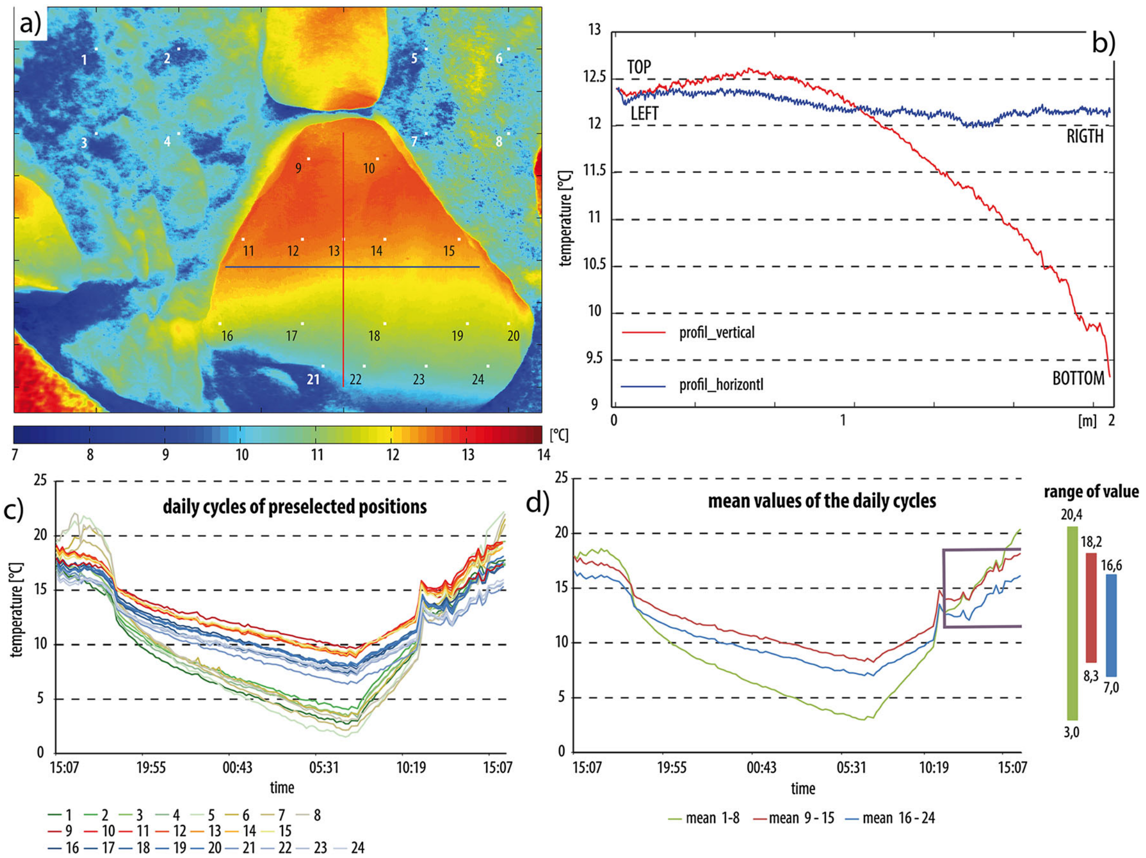

Figure 6. Results of the infrared measurments. (a) Average of the 24 h measurement (dots mark the positions for which the temperature fluctuations were analysed); (b) horizontal and vertical temperature profile (24 h mean); (c) daily temperature cycle at defined points; (d) averaged temperature cycles for certain areas (see text). This figure is available in colour online at wileyonlinelibrary.com/journal/espl

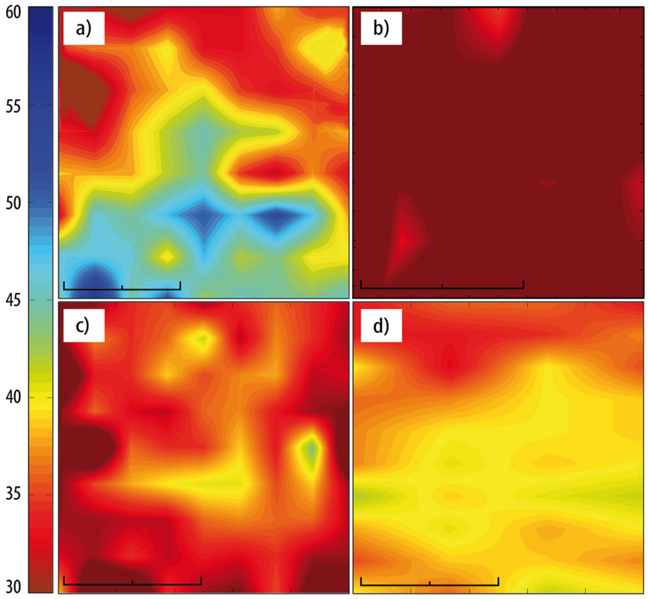

Figure 7. Results of the moisture meter measurements. (a) site 1 (west), inside the tafone; (b) site 1 (west), outside of the tafone; (c) site 1 (east), yellow-green patches correspond to small, shallow tafone; (d) inside the tafone at site 3. Relative readings from 0 (dry) to 100 (wet); the black bar denotes 2 m. This figure is available in colour online at wileyonlinelibrary.com/journal/espl

at site 1, a distinct trend was found with a clear decrease in the relative moisture values towards the top (Figure 7(a)). Thus, the lower area of the tafone seems to be moister than the upper part, which corresponds to the findings of the infrared monitoring. Similar patterns were found at site 3 (Figure 7(d)) even if the decrease of moisture with elevation is smaller at this site. Outside tafoni the rock was generally much drier and no differences in vertical direction were found (Figure 7(b)).

I-buttons

Similar to the IR results, the iButtons show a reasonably constant temperature difference between top and bottom of the tafone, and the largest amplitudes outside of the tafone (site 1, west-facing). The humidity data show a reverse diurnal variation with consistently higher relative humidity values at the bottom in comparison with the top (Figure 8(c)). The reason for this is the difference in temperature, as cooler air can absorb less moisture. Thus, to understand the process of water vapor diffusion relative humidity data are of limited benefit. The more significant water vapour pressure was computed from the temperature and relative humidity according to the Magnus formula (Defant and Defant, 1958). In terms of absolute vapour pressure it becomes clear that there are no humidity differences close to the surface inside (top or bottom) or outside the tafone (Figure 8(a)).

A pronounced diurnal cycle of temperature was detected only at depths of 3 and 20 cm while variations at 50 cm were just about 0.5°C per day (Figure 8(e)). Similarly, there is a clear diurnal cycle in both relative humidity and absolute vapour pressure at 3 cm depth while both parameters are constantly high at 50 cm depth.

Special attention was paid to the increase of vapour pressure with depth because vapour pressure differences trigger vapour diffusion. Between 50 and 3 cm, and from 3 cm to the surface, a vapour pressure gradient from the inner parts towards the surface was detected over the whole measurement period. Both curves depend on the time of the day: in the afternoon, the highest vapor deficit is located between 3 cm and the surface while in the morning hours, the maximum is between 50 cm and 3 cm, but there is no reversal at any time. This finding confirms that moisture is constantly transported from the interior to the surface, even if the transport in the gaseous phase is not able to move salts through the rock.

Relative humidity values from the iButtons can be converted into degree of (liquid) pore saturation via the laboratory-measured sorption isotherm (Figure 5). The average pore saturation in our measurement period was ~80% at 50 cm depth and ~10% at 3 cm.

Electrical resistivity tomography

Figure 9 displays the vertical and horizontal ERT profiles at site 1, site 3 and site 4 (Wenner and dipole–dipole measurements were combined in all cases). All extend to a depth of 30 cm to 40 cm inside the rock. The limits of resistivity for granite vary, depending on the textbook literature, between 10^3 and 10^5 ohm m (lower values for wet and higher values for dry rock). A similar range of values is found in all displayed profiles; the rather high maximum resistivity values can probably be attributed to the unusually high porosity (8%) of the Tafraoute granite. Because the structure of the rock appears to be

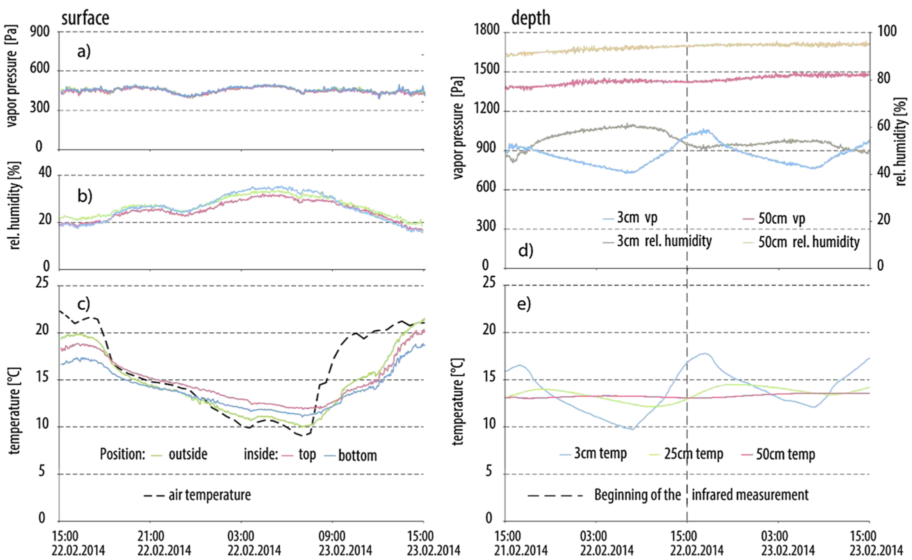

Figure 8. Results of iButtons measurement at site1 (west). This figure is available in colour online at wileyonlinelibrary.com/journal/espl

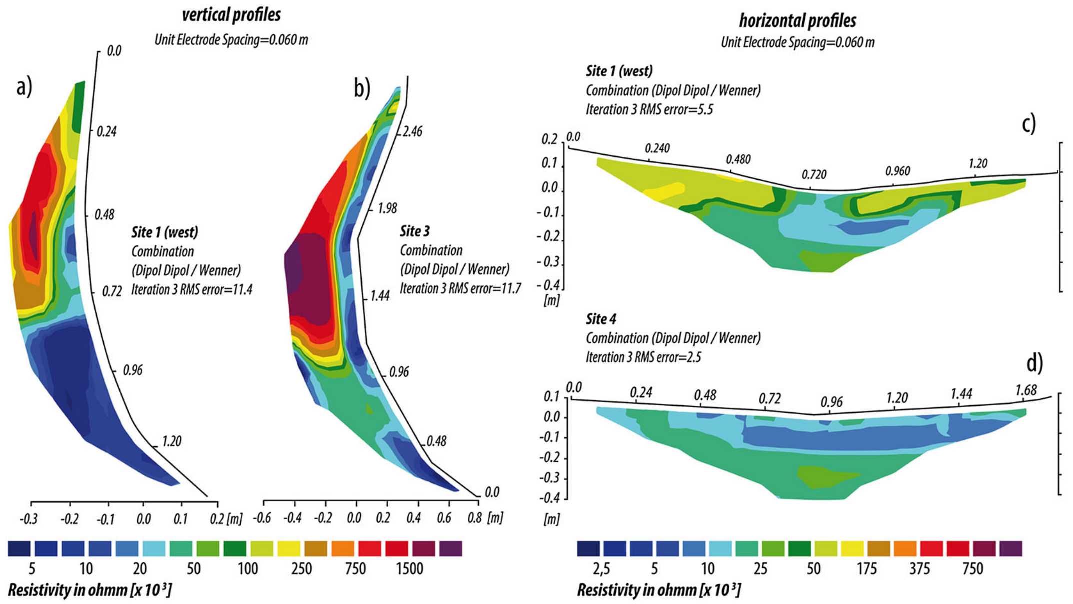

Figure 9. Results of ERT measurement at site 1 west (a), (c), site 3 (b) and site 4 (d). Each profile is combined from Wenner and dipole–dipole measurements; unit electrode spacing is 6 cm. This figure is available in colour online at wileyonlinelibrary.com/journal/espl

homogeneous and fractures are absent, it is likely that the measurements represent areas of different moisture and/or salt contents. Two general patterns can be seen in the vertical profiles (Figure 9(a), (b)). (1) Lower resistivity in the lower half of the profiles. For example, in the vertical profile of site 1, high values (>10^5 Ohmm) are found in the upper area and relatively low values (<10^3 ohm m) near the bottom (Figure 9(a)). As these resistivity patterns correspond well with the infrared and the moisture meter results, we assume that these low-resistivity zones represent wetter areas, possibly amplified by salts near the surface. (2) Higher resistivity deeper inside the rock, particularly in the upper half of the profiles. This contradicts the very clear results of the iButtons which indicate wetter conditions at depth. Thus, it is probable that the high conductivity/low resistivity recorded near the surface using ERT results from higher salt concentration not higher moisture levels.

Although the contrasts are smaller in the horizontal profile from site 1 (Figure 9(c)), it is evident that the edge of the tafone is slightly drier than the middle, and that there is a slight increase in moisture towards the inside of the rock. Similar patterns were also found in the horizontal profile at site 4 (Figure 9(d)) even if the resistivities are much lower. All measurements have a rather low RMS (root mean square; for the exact values see Figure 9) error and the DOI values (not displayed) do not exceed the threshold of 0.2 which indicates that the results reflect the real situation very well.

Drilling and sampling

Figure 10 displays the salt concentrations found in the samples of the four drill holes at site 1. Large quantities of sodium and sulfate are apparent particularly near the surface, along with other ions. At all measurement sites, except for the outer drill hole, salt concentrations increase towards the surface. Certain general patterns can be detected: first, a greater amount of salts are found close to the surface at all three sites within the tafone; second, concentrations of sulfate and sodium (to a lesser degree of chloride, bromide and magnesium) increase from the top towards the bottom of the tafone; and third, the increase of salt concentrations near the surface is not found in the outer drill hole (Figure 10(a)–(d)). These general findings are confirmed by the results of the drill dust conductivity measurements where maximum values are located at the surface and in the lower/moister area of the tafone (Figure 11). Similar patterns were also found within the tafoni borehole at site 4, but in this

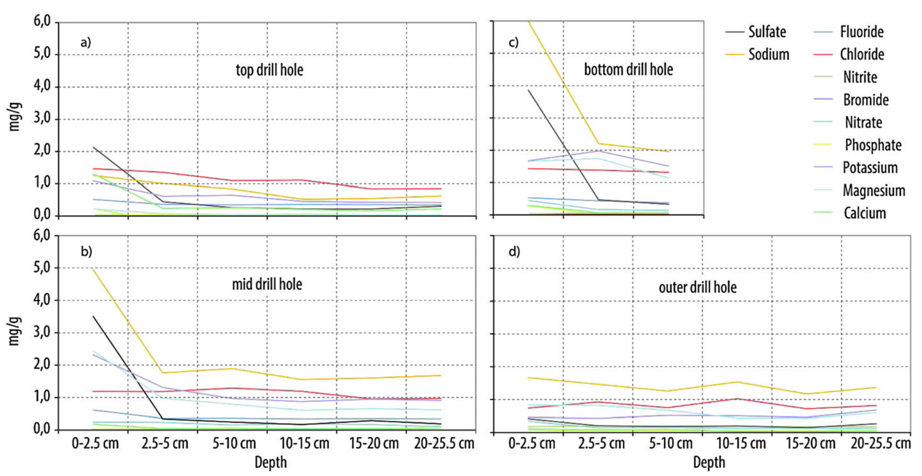

Figure 10. Concentrations of major ions in rock powder from different depths collected from the drillholes of site 1 (west). This figure is available in colour online at wileyonlinelibrary.com/journal/espl

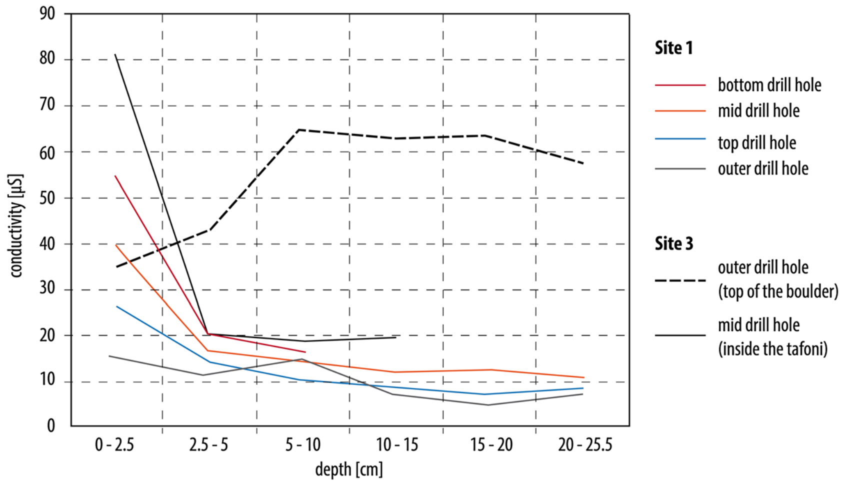

Figure 11. Conductivity values from rock powder from different depths collected from the drillholes in site 1 and site 3. This figure is available in colour online at wileyonlinelibrary.com/journal/espl

case the drill profile outside of the tafoni on the top of the boulder (which was vertical and not horizontal) is noticeably different as there is a significant increase of the values with increasing depth.

Because of the very similar distribution of sodium and sulfate it can be assumed with high probability that the dominant salt is sodium sulfate (as thenardite, the heptahydrite form or mirabilite; see Figure 13). According to Goudie (1977) and Goudie and Viles (1997), this salt is one of the most important agents of salt weathering especially in arid environments because of its high solubility in water, its ability to hydrate at humidities and temperatures frequently encountered in nature, and its long crystal habit.

Discussion

Utility of the techniques applied

The applied multi-method approach, combining relatively simple methods (drill dust sampling, hand held moisture meters) with novel and more sophisticated techniques (borehole humidity and temperature, ERT, thermography) has been demonstrated to provide useful data with which to gain insight into temperature, moisture and salt distribution. The data complement and support each other. Based on the measured data the following results can be summarized:

- Temperature amplitudes are subdued within tafoni compared with those on the surrounding rock faces (derived from: *infrared, iButtons*).
- Areas of elevated moisture content are found in the lower areas of the tafoni (*ERT, infrared, iButtons, moisture meter*); the rock inside the tafoni is moister than that outside (*moisture meter*). The humidity/absolute water vapour pressure increases with increasing rock depth (*iButtons*).
- Inside, but not outside, tafoni there is an accumulation of salts close to the rock surface (*drill dust sampling*). Salt concentrations increase towards the base inside tafoni (*drill dust sampling*).

Drill dust sampling turned out to be particularly helpful to clarify the salt concentration along depth profiles. This simple technique has rarely been carried out before (Viles and Goudie, 1992). Due to the high amount of material collected for analysis at each depth interval (drill diameter 18 mm) the results are likely to be highly representative. In many studies, only small amounts of weathered material from the surfaces within tafoni were collected (Mustoe, 1983; McBride and Picard, 2000). The drilling results were well worth the logistic effort because they give very clear evidence of the vertical and depth distribution of salts. Of course this method is not an option in many protected areas or conservation sites. The information can be used to cross-check the ERT results: in the current example it shows that high salt contents are a factor affecting conductivity/resistivity values only close to the surface (where counteracted by insufficient moisture) while resistivity patterns in the deeper subsurface must be caused by varying pore water content alone, as the salt levels are consistently low.

The measurements of borehole humidity have not been carried out before to our knowledge in comparable settings and they also delivered novel results, proving clearly that rock moisture (at the time of our measurements) increases with depth. As with drill dust sampling, the method depends on the availability of a battery-driven hammer drill and is likely to be more problematic on harder, less weathered granites. A longer measurement programme (months or years rather than days) would have been desirable and is planned for the future; it was not possible in the current field campaign for logistical reasons and because of vandalism. The cheap and easy-to-use hand held moisture meters were helpful to underpin the results of the ERT and IR measurements from which we infer spatial moisture distributions. However, the scatter of the measurements is very high and they are sometimes hardly reproducible; accordingly, anything more than a very rough, semi-quantitative orientation is not possible.

Finally, IR thermography (24 h monitoring) proved to be very helpful to gain high-resolution information on spatial and temporal patterning of surface temperatures and to delimit moister and drier areas. The consistent temperature difference between the upper and lower area within the west-facing tafone at site 1 clearly points to evaporative cooling and thus, to higher amounts of moisture towards the base. This process seems to be so strong that even the influence of direct radiation (west-facing, approx. from 16:00 to 17:30) is suppressed. An effect of higher emission at night can be ruled out because of the constant temperature difference throughout the 24 h period. As these assumptions are clearly confirmed by the results of other methods, IR thermography was shown to be a valid method to gain data on temperature and moisture distribution. However, short measurement times (or single shot images) are of very limited value.

Origin and distribution of salts

The results of our measurements show that moister areas near the surface also have a higher salt content, a correlation found in many publications on tafoni (Bradley *et al.,* 1978). The reason is that moisture is the agent of transport for dissolved salts. Possible sources of water that merit consideration include dew, fog, rain and groundwater, and two processes are responsible for the movement of moisture in the rock: capillary transport (which is also the main process of salt transport), and vapor diffusion which is responsible for the dehydration of rock. As dehydration is, in turn, responsible for the crystallization of salts the process of vapor diffusion has a great influence on the position of salts in the rock.

Huinink *et al.* (2004) tried to simulate water and salt movement within a developing tafone in a mathematical model. They regarded two different cases: a short drying period and a long one ($t=2000\Delta t$) and their results show that a long drying period is very important for the development of tafoni because there is ample time for salts to migrate to the slow-drying areas, following gradients of concentration. This mechanism is also held responsible for the tendency of tafoni to grow upward because 'most salt accumulates at the more sheltered (from the sun) part of the rock surface, having the lowest drying rates, given that the drying period in a wetting/drying cycle is long enough. Therefore, these parts weather faster than the exterior part and cavernous structures, e.g. Tafoni, develop.' (Huinink *et al.,* 2004, p.1231). This mechanism explains the tendency of tafoni to grow upward. From our own data (e.g. moisture meter) we are able to confirm that the interiors of tafoni dry more slowly than external rock faces and that salts are concentrated in these regions of slow drying (see salt sampling results). In contrast to Huinink *et al.* (2004), in our study site this area is located at the base and not in the upper parts of the tafoni. This might be due to the specific topographic situation at Tafraoute. In this case, we assume that under the rock tor at our main study site a lens of high soil moisture develops (Figure 12), a situation which may be different under isolated blocks or in higher positions of a rock wall.

The model outlined in Figure 12 is based on our findings from Tafraoute. One of the core questions is do water and salts, respectively, derive from the outside (fog, rain, dew, aeolian salt deposition) or from the inside (groundwater body) of the rock. We assume two possible pathways of salt enrichment. (1) Water (with salts) infiltrates from the top of the tor (red arrow) and from the relatively flat surrounding (blue arrow) and forms a body of +/− saturated rock under and within the tor. Due to evaporation and vapor pressure gradients, capillary water is sucked to the surface and salts are precipitated near the surface. The main area of salt enrichment at site 1 is the basal area of the tafone due to the proximity to the saturated zone (primary path). (2) Salts may be also deposited with aeolian dust. On smooth rock faces without tafoni, large portions of these salts are probably washed off, while inside the tafoni they remain at the rock surface, or are dissolved during dewfall events and infiltrate into the outermost centimeters of rock (secondary path). Both outlined mechanisms lead to salt concentration in sheltered places and near the base of the rock. This model contradicts the work of Bradley *et al.* (1978) and the model of Huinink *et al.* (2004) both of which hypothesized that salts (as well as moisture) should be primarily found in the upper, protected areas of tafoni while the lower parts of the tafoni are probably more exposed to wind, rain and radiation. A reason for the unexpectedly high salt and moisture content in the lower parts of the investigated tafoni at Tafraoute could be that these areas receive a higher input of atmospheric salts. However, if this was the case a markedly higher amount of salt would have to be expected outside of the tafoni which is not the case (with the notable exception of the roof of tafone 3, see below). Thus, for the inside of the tafoni it is more likely that the salts originate from a water body (or area of higher humidity) inside the rock from where they are transported by capillary transport towards the surface. This would mean that tafoni in comparable settings mainly develop near the base of boulders and tors and up to the assumed level of capillary rise which is, in fact, often the case.

The salt concentration at the top of the boulder at site 3 shows a significant increase in salt concentration with depth (Figure 11, dashed line) and thus differs from the profiles inside the tafoni at sites 1 and 3. A reason for this could be the combination of rain and rapid dehydration caused by the high direct radiation. Due to fast drying after rain, atmospheric salts crystallize at a certain depth. During subsequent rain events the salts are successively transported to greater depths (Figure 12, red arrow). This pathway of salt displacement would explain the development of Tafoni in higher areas of tors and their growth upwards. This assumption is, however, supported only by one measurement and is therefore speculative.

Implications for salt weathering

Textbook concepts of salt weathering assume that damage is induced by: (i) crystallization pressure (Correns, 1949; Scherer, 1999); (ii) stresses induced by crystal hydration (Mortensen, 1933; Winkler and Wilhelm, 1970); and (iii) a differential thermal expansion of salts (Cooke and Smalley, 1968; Charola, 2000). The borehole humidity data derived from the iButtons can be used to underpin these assumptions. With high probability, the dominant salt at our study sites is sodium sulfate which occurs in nature in two varieties: the water-free thenardite and the hydrated variety mirabilite. A third metastable variety which might crystallise on cooling to around 10°C was reported on by

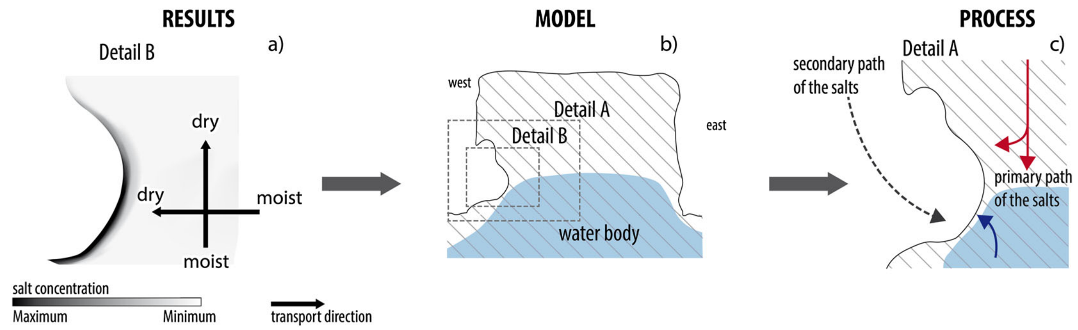

Figure 12. (a) Salt concentrations and moisture gradients according to the measurements; (b) supposed distribution of saturated rock; (c) supposed migration paths of salts. This figure is available in colour online at wileyonlinelibrary.com/journal/espl

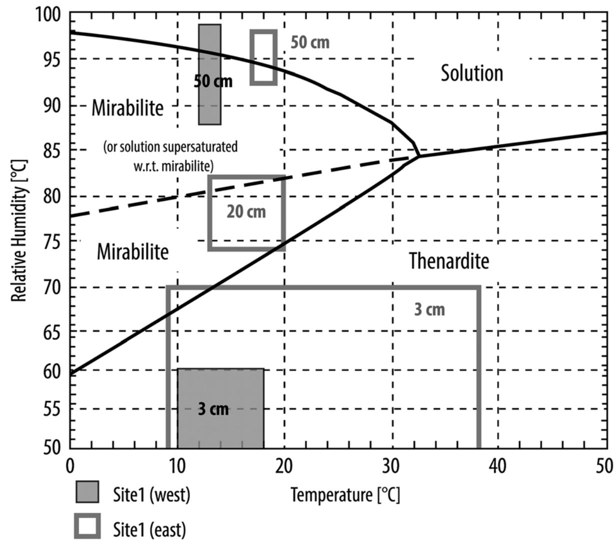

Figure 13. Phase diagram for sodium sulfate. The continuous lines indicate the limits between the stable phases. The discontinuous line corresponds to a solution in metastabile eqilibrium with respect to thenardite and supersaturated with respect to mirabilite (Tsui *et al.*, 2003). The grey rectangles (site1 west) indicate the measured T/H data at 50 and 3 cm depth from 21/2/14 to 23/2/14; the rectangles (site 1 east) indicate the measured T/H data at 50, 20 and 3 cm depth from 14/2/14 to 24/2/14, respectively.

Hall and Hamilton (2008). Assuming that crystallization pressure is the primary source of damage, Rodriguez-Navarro *et al.* (2000) argued that precipitation of thenardite rather than mirabilite may be responsible for damage from sodium sulfate, particularly in situations of constant capillary rise.

As Figure 13 shows, the results of our micro-climatic measurements suggest that due to higher humidities found in the pores, sodium sulfate at a depth of 50 cm should occur in dissolved form (or supersaturated with respect to mirabilite). Just below the surface (3 cm), however, the anhydritic thenardite should prevail. Due to the short measurement period the conclusions are speculative; yet it can be assumed that the mirabilite–thenardite transition frequently occurs at this depth range, either by the capillary transport towards the surface and crystallization, or because of changing weather conditions when the surface is wetted or the drying front propagates deeper into the rock in summer. These patterns were also found at the east side of site 1 and at site 5 and 6 (not displayed).

Conclusions

To sum up, the following conclusions can be drawn from the measurements presented here:

- The combination of high-resolution temperature, moisture and salt measurements enables valuable insights into tafoni formation at our study site in Tafraoute, Morocco. The results derived from very different techniques (IR, T and H sensors, ERT, hand held moisture meters, drill dust sampling) mutually support one another.
- Our results confirm that moisture and salt concentration are elevated inside tafoni compared with the surrounding rock.
- A clear correlation was found between moisture and salt contents. Within a tafone, areas of higher humidity also display increased salt concentration near the surface. ERT reacts to both parameters; the least resistive areas are those with high levels of both moisture and salts.
- Our measurements clearly show a significant accumulation of salts close to the rock surface in tafoni, but not on the surrounding rock surfaces. These findings appear to be consistent with the model of Huinink *et al.* (2004) which predicts enhanced salt deposition in zones of low drying rates.
- Salts and moisture at our sites were concentrated near the base of tafoni which has, to our knowledge, not been reported in the literature before. We assume that the reason is a saturated pore water body around the base of rock tors which might be common in most places other than highly free-standing boulders.
- The measured T/H-values indicate that salts (in this case sodium sulfate) occur in various phases which implies frequent phase changes from thenardite to mirabilite and vice versa.
- Two pathways of salt transport in and around tafoni are assumed based on the data: infiltration with rainfall on the top and around tors and boulders, and capillary rise from saturated pore water bodies to the surface. Direct dry deposition is probably of subordinate importance.

References

Angelopoulos MC, Pollard WH, Couture NJ. 2013. The application of CCR and GPR to characterize ground ice conditions at Parsons Lake, Northwest Territories. *Cold Regions Science and Technology* **85**: 22–33.

Barbey P, Oberli F, Burg J-P, Nachit H, Pons J, Meier M. 2004. The Palaeoproterozoic in western Anti-Atlas (Morocco): a clarification. *Journal of African Earth Sciences* **39**: 239–245.

Benziane F. 2007. Lithostratigraphie et évolution géodynamique de l'anti-Atlas (Maroc) du paléoprotérozoïque au néoprotérozoïque: exemples de la boutonnière de Tagragra Tata et du Jebel Saghro. Doctoral thesis, Université Savoie, France.

Bradley WC, Hutton JT, Twidale CR. 1978. Role of salts in development of granitic tafoni, South Australia. *The Journal of Geology* **86**(5): 647–654.

Brandmeier M, Kuhlemann J, Krumrei I, Kappler A, Kubik PW. 2011. New challenges for tafoni research: a new approach to understand processes and weathering rates. *Earth Surface Processes and Landforms* **36**: 839–852.

Boelhouwers J, Jonsson M. 2013. Critical Assessment of the 2°C min^{-1} threshold for thermal stress weathering. *Geografiska Annaler: Series A, Physical Geography* **95**(4): 285–293.

Budzier H, Gerlach G. 2010. *Thermische Infrarot Sensoren*. Weinheim: Wiley-VCH.

Campbell SW. 1999. Chemical weathering associated with tafoni at Papago Park, Central Arizona. *Earth Surface Processes and Landforms* **24**: 271–278.

Charola AE. 2000. Salts in the deterioration of porous materials: an overview. *Journal of the American Institute for Conservation* **39**: 327–343.

Cooke RU, Smalley IJ. 1968. Salt Weathering in Deserts. *Nature* **220**: 1226–1227.

Correns CW. 1949. *Einführung in die Mineralogie (Kristallographie und Petrologie)*. Springer-Verlag: Berlin-Göttingen-Heidelberg 414 S., 405 Abb., 1 Tafel. Geh. DM 38.—, geb. DM 41.60.

Defant A, Defant F. 1958. *Physikalische Dynamik der Atmosphäre*. Frankfurt: Akademische Verlagsgesellschaft.

Dionisio A, Martinho E, Grangeia C, Almedia F. 2013. Examples of the use of non-invasive techniques for the evaluation of stone decay in Portugal. *Key Engineering Materials* **548**: 239–246.

Doehne E. 2002. Salt weathering: a selective review. In natural stone, weathering phenomena, conservation strategies and case studies. *Geological Society Special Publications* **205**: 51–64.

Dorn RI, Gordon SJ, Krinsley D, Langworthy K. 2013. Nanoscale: Mineral Weathering Boundary. In *Treatise on Geomorphology*. Academic: Oxford.

Eklund JA, Zhang H, Viles HA, Curteis T. 2013. Using handheld moisture meters on limestone: factors affecting performance and guidelines for best practice. *International Journal of Architectural Heritage* **7**: 207–224.

Franzen C, Mirwald PW. 2009. Moisture sorption behaviour of salt mixtures in porous stone. *Geochemistry* **69**: 91–98.

French HM, Guglielmin M. 2000. Cryogenic weathering of granite, northern Victoria land, Antarctica. *Permafrost and Periglacial Processes* **11**: 305–314.

Goudie AS. 1977. Sodium sulphate weathering and the disintegration of Mohenjo-Daro, Pakistan. *Earth Surface Processes and Landforms* **2**(1): 75–86.

Goudie AS, Viles HA. 1997. *Salt Weathering Hazards*. Wiley: Chichester/ New York.

Gaussorgues G, Chomet S. 1993. *Infrared Thermography*. Springer Verlag. ISBN:0412479001.

Gruner K. 2004. *Grundlagen der berührungslosen Temperaturmessung „Strahlungsthermometrie". Revision B1. 12/2004*. Raytek Europazentrale: RaytekGmbH, Berlin.

Hall C, Hamilton A. 2008. The heptahydrate of sodium sulfate: does it have a role in terrestrial and planetary geochemistry? *Icarus* **198**: 277–279.

Hall K. 1986. Rock moisture content in the field and the laboratory and its relationship to mechanical weathering studies. *Earth Surface Processes and Landforms* **11**: 131–142.

Hall K. 1991. Rock moisture data from the Juneau Icefield (Alaska) and its significance for mechanical weathering studies. *Permafrost and Periglacial Processes* **2**: 321–330.

Hall K, André MF. 2001. New insights into rock weathering from high-frequency rock temperature data: an Antarctic study of weathering by thermal stress. *Geomorphology* **41**: 23–35.

Hall K, Meiklejohn I, Arocena J. 2007. The thermal responses of rock art pigments: implications for rock art weathering in southern Africa. *Geomorphology* **91**: 132–145.

Hassenforder B. 1985. Les mylonites de la zone de faille ductile panafricaine des Ameln (Kerdous, Anti-Atlas occidental, Maroc). Une analyse pétrostructurale de la déformation. *Sciences géologique Strasbourg* **38**: 215–226.

Hassenforder B. 1987. La tectonique panafricaine et varisque de l'Anti-Atlas dans le massif du Kerdous (Maroc). Doctoral Thesis, University of Strasbourg.

Hilbich C, Marescot L, Hauck C, Loke MH, Mäusbacher R. 2009. Applicability of electrical resistivity tomography monitoring to coarse blocky and ice-rich permafrost landforms. *Permafrost and Periglacial Processes* **20**(3): 269–284.

Huinink HP, Pel L, Kopinga K. 2004. Simulating the growth of Tafoni. *Earth Surface Processes and Landforms* **29**: 1225–1233.

James WL. 1963. *Electric moisture meters for wood*. US Forest Service: Madison, WI.

Kearey P, Brooks M, Hill I. 2002. *An Introduction to Geophysical Exploration*. Blackwell Science: Malden.

Krus M. 1995. Feuchtetransport- und Speicherkoeffizienten poröser mineralischer Baustoffe. Theoretische Grundlagen und neue Messtechniken. Doctoral thesis, Universität Stuttgart.

Marescot L, Loke MH, Chapellier D, Delaloye R, Lambiel C, Reynard E. 2003. Assessing reliability of 2D resistivity imaging in mountain permafrost studies using the depth of investigation index method. *Near Surface Geophysics* **1**(2): 57–67.

Martinho E, Alegria F, Dionisio A, Grangeia C, Almeida F. 2012. 3D-resistivity imaging and distribution of water soluble salts in Portuguese Renaissance stone bas-reliefs. *Engineering Geology* **141–142**: 33–44.

Materialarchiv. 2014. http://www.materialarchiv.ch/detail/43#/detail/43/granit (accessed 05/03/2015)

Matsukura Y, Takahashi K. 2000. A new technique for rapid and non-destructive measurement of rock-surface moisture content; preliminary application to weathering studies of sandstone blocks. *Engineering Geology* **55**: 113–120.

Maurício A, Figueiredo C, Aires-Barros L. 2006. Monitoring salt systems in monument stones: comparing two electrochemical methods. In *Proceedings of the International Conference on Heritage, Weathering and Conservation* (HWC-2006). Taylor & Francis: London.

McBride EF, Picard MD. 2000. Origin and development of tafoni in Tunnel Spring Tuff, Crystal Peak, Utah, USA. *Earth Surface Processes and Landforms* **25**(8): 869–879.

Mellor A, Short J, Kirkby SJ. 1997. Tafoni in the El Chorro area, Andalucia, southern Spain. *Earth Surface Processes and Landforms* **22**: 817–833.

Mol L, Viles HA. 2010. Geoelectric investigations into sandstone moisture regimes: Implications for rock weathering and the deterioration of San Rock Art in the Golden Gate Reserve, South Africa. *Geomorphology* **118**: 280–287.

Mol L, Viles HA. 2012. The role of rock surface hardness and internal moisture in tafoni development in sandstone. *Earth Surface Processes and Landforms* **37**: 301–314.

Mortensen H. 1933. Die 'Salzsprengung' und ihre Bedeutung für die regional klimatische Gliederung der Wüsten. *Petermanns Geographische Mitteilungen* **79**: 130–135.

Mottershead DN, Pye K. 1994. Tafoni on Coastal Slopes, South Devon, UK. *Earth Surfaces Processes and Landforms* **19**: 543–563.

Mustoe GE. 1983. Cavernous weathering in the Capitol Reef Desert, Utah. *Earth Surface Processes and Landforms* **8**: 517–526.

Oldenburg DW, Li Y. 1999. Estimating depth of investigation in DC resistivity and IP surveys. *Geophysics* **64**(2): 403–416.

Plagge R, Funk M, Scheffler G, Grunewald J. 2006. Experimentelle Bestimmung der hygrischen Sorptionsisotherme und des Feuchtetransportes unter instationären Bedingungen. *Bauphysik* **28**(2): 81–87.

Rodriguez-Navarro C, Doehne E, Sebastian E. 1999. Origins of honeycomb weathering: the role of salts and wind. *Geological Society of America Bulletin* **111**: 1250–1255.

Rodriguez-Navarro C, Doehne E, Sebastian E. 2000. How does sodium sulfate crystallize? Implications for the decay and testing of building materials. *Cement and Concrete Research* **30**(10): 1527–1534.

Sass O. 2003. Moisture distribution in rockwalls derived from 2D-resistivity measurements. Geophysical applications in geomorphology, Zeitschrift für Geomorphologie Suppl. **132**: 51–69.

Sass O. 2005. Rock moisture measurements: techniques, results, and implications for weathering. *Earth Surface Processes and Landforms* **30**: 359–374.

Sass O, Viles HA. 2010a. Wetting and drying of masonry walls: 2D-resistivity monitoring of driving rain experiments on historic stonework in Oxford, UK. *Journal of Applied Geophysics* **70**: 72–83.

Sass O, Viles HA. 2010b. 2D resistivity surveys of the moisture contents of historic limestone walls in Oxford, UK: implications for understanding catastrophic stone deterioration. In *Limestone in the Built Environment: Present Day Challenges for Preservation of the Past*, Smith BJ, Gomez Heras M, Viles HA, Cassar J (eds). *Geological Society of London, Special Publication* **331**: 237–249.

Scherer G. 1999. Crystallization in pores: Princeton University, CEE/PMI, Eng. Quad. E-319, Princeton, NJ 08544, USA. *Cement and Concrete Research* **29**: 1347–1358.

Schrott L, Sass O. 2008. Application of field geophysics in geomorphology: Advances and limitations exemplified by case studies. *Geomorphology* **93**: 55–73.

Schuster N, Kolobrodov VG. 2000. *Infrarotthermographie*. Weinheim: WILEY-VCH.

Service Géologique du Maroc. 1985. Carte géologique du Maroc. Échelle: 1/1000000, Rabat.

Shannon HR, Sigda JM, Van Dam RL, Hendrickx JMH, McLemore VT. 2005. Thermal Camera Imaging of Rock Piles at the Questa Molybdenum Mine, Questa, New Mexico. In Proceedings of a Joint Conference of American Society of Mining and Reclamation (ASMR) 22nd Annual National Conference.

Skaar C. 1988. *Wood–Water Relations*. Springer-Verlag: Berlin.

Soulaimani A, Piqué A. 2004. The Tasrirt structure (Kerdous inlier, Western Anti-Atlas, Morocco): a late Pan-African transtensive dome. *Journal of African Earth Sciences* **39**(3): 247–255.

Strini A, Guglielmin M, Hall K. 2008. Tafoni development in a cryotic environment: an example from Northern Victoria Land, Antarctica. *Earth Surface Processes and Landforms* **33**: 1502–1519.

Sumner PD, Hall KJ, van Rooy JL, Meiklejohn KI. 2009. Rock weathering on the eastern mountains of Africa: Review and insight from case studies. *Journal of African Earth Sciences* **55**: 236–244.

Testo AG (ed). 2006. Leitfaden zur Infrarot-Messtechnik. http://www.testo.com (accessed 06/2011).

Teza G, Marcato G, Castelli E, Galgaro A. 2011. IRTROCK: a MATLAB toolbox for contactless recognition of surface and shallow weakness of a rock cliff by infrared thermography. *Computer & Geosciences* **45**: 109–118.

Tsui N, Flatt RJ, Scherer GW. 2003. Crystallization damage by sodium sulphate. *Journal of Cultural Heritage* **4**: 109–115.

Turkington AV, Martin E, Viles HA, Smith BJ. 2003. Surface change and decay of sandstone samples exposed to a polluted urban atmosphere over a six-year period: Belfast, Northern Ireland. *Building and Environment* **38**: 1205–1216.

Turkington AV, Paradise TR. 2005. Sandstone weathering: a century of research and innovation. *Geomorphology* **67**(1): 229–253.

Turkington AV, Phillips JD. 2004. Cavernous weathering, dynamical instability and self-organization. *Earth Surface Processes and Landforms* **29**: 665–675.

Viles HA, Goudie AS. 1992. Weathering of limestone columns from the Weymouth seafront, England. In Proceedings of the 7th International Congress on Deterioration and Conservation of Stone, Lisbon, June 1992.

Winkler EM, Wilhelm EJ. 1970. Salt burst by hydration pressures in architectural stone in urban atmosphere. *Geological Society of America Bulletin* **81**(2): 567–572.